# NUCLEAR MAGNETIC RESONANCE SPECTROSCOPIC AND COMPUTER-SIMULATED STRUCTURAL ANALYSES OF A HEPTAPEPTIDE SEQUENCE FOUND AROUND THE *N*-GLYCOSYLATION SITE OF A PROLINE-RICH GLYCOPROTEIN FROM HUMAN PAROTID SALIVA

R. E. LOOMIS,* K. K. BHANDARY,‡ C.-C. TSENG,* E. J. BERGEY,* AND M. J. LEVINE*
**State University of New York at Buffalo, School of Dental Medicine, Department of Oral Biology, Buffalo, New York 14214; and ‡Biophysics Department, Roswell Park Memorial Institute, Buffalo, New York 14263*

ABSTRACT The proline-rich glycoprotein from human parotid saliva has a common heptapeptide sequence around four of six *N*-glycosylation sites (Maeda, N., H. S. Kim, E. A. Azen, and O. J. Smithies, 1985, *J. Biol. Chem.*, 20:11123–11130). A synthetic model of the heptamer protein sequence, $NH_2$-Q(1)-G(2)-G(3)-N(4)-Q(5)-S(6)-Q(7)-$CONH_2$, was examined by nuclear magnetic resonance (NMR) spectroscopy and the ECEPP/2-VAO4A (Empirical Conformation Energy Program for Peptides) energy minimization computer algorithm (Scheraga, H. A., 1982, Quantum Chemistry Program Exchange, 454; Powell, M. J. D., 1964, Quantum Chemistry Program Exchange, 60). The NMR spectrum was almost completely assigned in dimethylsulfoxide-$d_6$ (DMSO), and the amide chemical shift temperature dependence, $\phi$ dihedral angles, and $\chi_1$ rotamer populations elucidated. These data indicated that a significant population of the heptamer could exist as a type I $\beta$-turn [4 → 1 between Q(5) and G(2)] and/or a type II′ $\beta$-turn [4 → 1 between (Q)5 and G(2) and/or a $\gamma$-turn [3 → 1 between Q(5) and G(3)] with the amino acid $\chi_1$ torsion angles weighted toward the *gauche*$^-$ conformation. Starting from these three possible conformations, the ECEPP/2-VAO4A rigid geometry energy minimization program was used to find the localized predominant *in vacuo* structures of this heptapeptide sequence. The type II′ $\beta$-turn conformation best fits the data based on internuclear hydrogen-bonding distances, minimum potential energy considerations, and the NMR parameters.

## INTRODUCTION

The proline-rich glycoprotein from human parotid saliva (PRG) is a 36.4-kD glycoprotein for which amino acid sequence data (1–3) and carbohydrate primary structure (4) have been reported. The biological functions of this macromolecule include participation in the formation of an acquired enamel film or "pellicle" on the tooth's surface (5, 6), action as a masticatory lubricant (7), and binding to the lectin-like components on the surface of oral streptococci (8–10). We have begun to probe the relationships between the biological functions of this molecule and its solution-state conformation using a variety of biophysical techniques. Nuclear magnetic resonance (NMR) relaxation studies, circular dichroism data, fluorescence spectroscopy experiments, thermodynamic calculations, and semiempirical structure predictions have collectively suggested that PRG has a flexible protein structure with a large number of turn sequences (11, 12). The carbohydrate moieties in PRG have been shown to be responsible for masticatory lubrication (7). Also, the complexation of PRG with oral bacteria is believed to be predicated largely upon the presence of the oligosaccharides (10).

The present study concerns itself with the secondary structure of the protein backbone in the vicinity of the *N*-glycosylation sites on PRG. Out of six locations, four have the peptide sequence Q(1)-G(2)-G(3)-N(4)-Q(5)-S(6)-Q(7), while a fifth has Q(7) replaced by H(7). In each case glycosylation occurs at N(4). We report here the use of a synthetic heptapeptide model of this region for two-dimensional NMR and computer-assisted energy minimization conformational analyses. Ultimately, knowledge of the conformational topography of key domains in salivary macromolecules could provide insights for the development of selective artificial salivas, to be custom designed for a patient's particular needs.

## MATERIALS AND METHODS

### Materials

The model heptapeptide was custom synthesized and purchased from OCS Laboratories, Denton, TX. The amino acid composition was verified

using previously published methods (4) on a 6300 High Performance Analyzer (Beckman Instruments, Inc., Palo Alto, CA). Primary amino acid sequence was verified on a 890 Automated Amino Acid Sequencer (Beckman Instruments, Inc.) Both our results and those of the manufacturer indicated the correct amino acid sequence with a minimum of 98% purity.

The peptide was taken up in deionized-distilled water and passed over a 24 × 1.5-cm hydrogen-form 200–400 mesh Chelex-100 (Bio-Rad Laboratories, Richmond, CA) column to eliminate divalent metal ion contamination. The pH of the resulting solution was adjusted to 7.4. The lyophilized material was then used for NMR analyses in perdeuterated dimethylsulfoxide (DMSO) dried over 3-Å molecular sieve.

## NMR Methods

NMR data were collected and processed on a Nicolet/General Electric Corporation 8.45 Tesla narrow bore spectrometer equipped with a Nicolet/General Electric Corporation 1180E computer and a dual 50 megabyte cartridge disk drive system (model 9427H, Control Data Corp., Minneapolis, MN). Coupling constant analyses were performed with the NMRSIM spectral simulation program on the Nicolet/General Electric Corporation 1180E computer. The peptide was examined at a concentration of 6.4 mM in DMSO at a constant temperature of 30 ± 0.2°C maintained by a Nicolet/General Electric Corporation variable temperature control assembly. A spectrometer carrier frequency of 361.074602 MHz for protons was used. The two-dimensional J-correlated (COSY) spectra were obtained using the following pulse sequence (13)

$$(\Delta_1 - \pi/2 - \Delta_2 - t_1 - \pi/2 - \Delta_2 - t_2)_n. \qquad (1)$$

The transmitter and receiver radio frequencies were phase cycled to eliminate spectral artifacts (14). A delay $\Delta_2$ value of 230 ms was used to emphasize selected five-bonded couplings (15). Two-dimensional Nuclear Overhauser Effect spectroscopy (NOESY) experiments were attempted using the pulse sequence of Baumann et al. (16). All two-dimensional NMR spectra had the following parameters in common: quadrature phase detection in both the $\omega_1$ and $\omega_2$ dimensions, a sweep width of ±3012.04 Hz, 3 dB of Butterworth filter attenuation, 64 transients collected per data set, a relaxation delay ($\Delta_1$) of 1.5 s to allow maximum practical time for recovery of $T_1$ to thermal equilibrium, 8.5 $\mu$s $\mu/2$ pulse width, and a final symmetrized (17) data matrix size of 512 × 512 points. Free induction decays were apodized by multiplication with the first $\pi$ radians of a sine bell function. High resolution one-dimensional NMR spectra were collected in 8 K data blocks and zero-filled three times to 32 K using 500 transients. Phase cycling was incremented by $\pi/2$ radians over four steps to complete the basic quadrature experiment. All other parameters were the same as in the two-dimensional NMR experiments. Chemical shifts are reported in parts per million (ppm) downfield from internal 2,2-dimethyl-2-silapentane-5-sulfonate (DSS).

## Computational Methods

Computer analysis of the heptapeptide bond angles was carried out using the ECEPP/2-VAO4A (Empirical Conformational Energy Program for Peptides) rigid geometry energy minimization program (18, 19) on a VAX-11/785 computer system at SUNY, Buffalo (Digital Equipment Corp.) using the VMS 4.1 operating system. Molecular models were initially drawn with the ORTEP thermal ellipsoid plot program (20) on the Roswell Park Memorial Institute UNIVAC computer (model 90/80-4; Sperry Corp., Sperry Univac, Blue Bell, PA) utilizing the VS9 operating system and six megabytes of virtual access memory. The UNIVAC computer was interfaced to a video graphics display system (model 4006-1; Tektronix, Beaverton, OR) and an interactive digital plotter (model 4662; Tektronix). Perspective color renderings of the ORTEP plots were generated by Oceana, Buffalo, New York. Internuclear distances were calculated by a local FORTRAN program written for the UNIVAC computer (Kartha, G., unpublished data). Evaluation of $\chi_1$ rotamer populations was accomplished using matrix algebra on a 15C calculator (Hewlett-Packard Co., Palo Alto, CA). All other calculations were performed by simple programs written for the Hewlett-Packard 15C calculator.

# RESULTS AND DISCUSSION

## NMR Heptapeptide Chemical Shift and Temperature Dependence Analysis

The stacked COSY plot for the proton NMR spectrum of the heptapeptide is illustrated in Fig. 1. The corresponding contour plot (with the one-dimensional spectrum obtained by projection through the $\omega_1$ dimension plotted above the contour map) is shown in Fig. 2. Chemical shifts were assigned using the modified COSY technique as described by Wynants et al. (15). Each type of spin system was readily distinguished with $\Delta_2$ set to 0 ms. To lift the degeneracy between groups of similar spin systems, $\Delta_2$ was set to 230 ms to visualize 5-bonded peptide backbone amide proton connectivities. In this way N(4) protons were used as unique atomic centers and the amide proton chemical shifts of G(3) and Q(5) were assigned. S(6) also gave unique chemical shift values, which established the assignment of the Q(7) amide proton and confirmed that of Q(5). The process of elimination gave the chemical shift assignment for the G(2) amide proton. Once the specific origin (within individual spin-systems) for each 3-bonded NH—$C^\alpha H^\alpha$ proton connectivity was established (again using COSY with $\Delta_2$ set to 0 ms), the $C^\alpha H^\alpha$—$C^\beta H^\beta$ and $C^\beta H^\beta$—$C^\gamma H^\gamma$ connectivities were evaluated. This approach allowed assignment of all the protons in the heptapeptide except for the amide protons on the amino acid functional groups and the $NH_2$ and COOH terminals. In these cases the COSY crosspeaks were either too close to the diagonal and/or were severely overlapped such that ambiguities in assignments arose. Similarly, the amino acid functional groups for the glycines (i.e., single protons) were indistinguishable from their corresponding $C^\alpha H^\alpha$ protons.

The dependence of amide and $C^\alpha H^\alpha$ proton chemical shifts on temperature between 293 K and 328 K at 5 K intervals was determined. These data were extracted from the high-resolution one-dimensional NMR experiments. Plots of chemical shift versus temperature for the amide and $C^\alpha H^\alpha$ protons are presented in Fig. 3. The chemical shift and $\Delta\delta/\Delta T$ parameters are listed in Table I. These data indicate that with the exception of Q(5), the plots were monotonic and gave rise to $\Delta\delta/\Delta T$ values with relatively large, negative slopes. The Q(5) $\Delta\delta/\Delta T$ constant, however, is small and positive. Since the $C^\alpha H^\alpha$ proton chemical shifts varied linearly with temperature, no apparent change in structure (on the NMR time scale) occurred over the temperature range examined here (21). The data thus imply that the Q(5) amide proton is involved in an intramolecular hydrogen bond (22, 23).

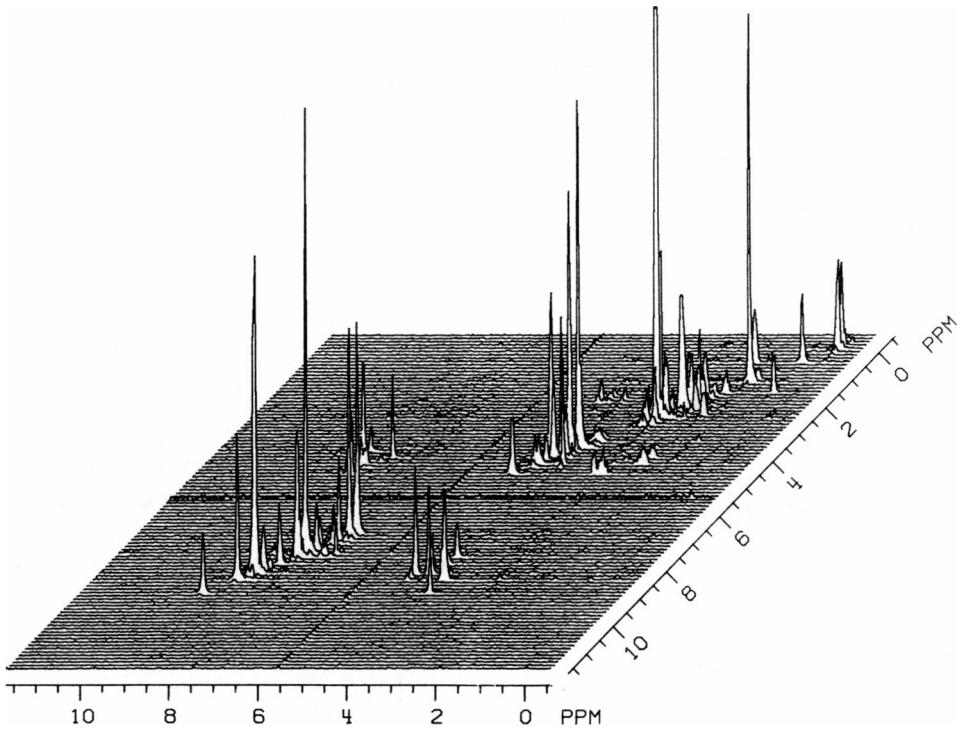


FIGURE 1 The 360 MHz $^1$H-NMR COSY stacked plot of the $NH_2$-Q(1)-G(2)-G(3)-N(4)-Q(5)-S(6)-Q(7)-$CONH_2$ heptapeptide sequence around the *N*-glycosylation site of the proline-rich glycoprotein from human parotid saliva.

## NMR Analysis of the Heptapeptide $\phi$ Torsion Angles

The definitions of the $\phi$ and $\chi_1$ dihedral angles are illustrated in Fig. 4 (also see first footnote to Table III). These angles and specifications of rotamer populations follow the nomenclature of IUPAC-IUB (24) and Bystrov (25). Also, Fig. 4 C shows the general form of the Karplus Equation (26, 27) and the standard method used to convert between $\theta$ and $\phi$. Fig. 5 is a plot of the Karplus Equation using the **A, B,** and **C** coefficient values of 6.4, −1.4, and 1.9, respectively, suggested by Pardi et al. (28).

Table II lists the $^3J_{NH,C^\alpha H^\alpha}$ coupling constants obtained from the high-resolution one-dimensional NMR spectra of the heptamer at 30° C, and the corresponding values of $\theta$ and $\phi$. There are two solutions for $\phi$ at each $\theta$ value since, as can be seen in Fig. 5, the Karplus Equation follows a sinusoidal path. Generally, one thus obtains four possible solutions to $\phi$ for each coupling constant value. As stated in the fourth footnote of Table II, the $^3J_{NH,C^\alpha H^\alpha} = 8.09$ value for N(4) is a unique situation since there is only one possible value for $\theta$ (based on the plot in Fig. 5). Inspection of the two corresponding $\phi$ values in Table II reveals that the solutions for N(4) are −148.4° and −91.6°. The −148.4° value is quite distant from any regular secondary structure one might expect for a small linear peptide, while the −91.6° solution is very near the $\phi_{i+2} = -90°$ or −80° value one would expect for the second corner position of either a type I or type II′ $\beta$-turn, respectively (29, 30). Unfortunately the G(3) $^3J_{NH,C^\alpha H^\alpha}$ coupling constant is anomalous in that $C^\alpha H^\alpha$ and the R = H functional group are indistinguishable, therefore, we can not directly determine $\phi_{i+1}$. The Q(5), S(6), and Q(7) $\phi$ values would most likely give rise to an extended chain (e.g., $\phi = -180°$) or be part of a $3_{10}$- or $\alpha$-helix (e.g., $\phi = -60°$ or −57°, respectively). The type III $\beta$-turn is actually one turn of a $3_{10}$-helix with all the residues existing with the same dihedral angles (e.g., $\phi = -60°$) (29), therefore this could be one possible conformation. However, since both solutions to the N(4) $\phi$ torsion angle are quite removed from −60°, a more likely conformation for this model heptapeptide would be a type I or type II′ $\beta$-turn with a 4 → 1 intramolecular hydrogen bond between Q(5) and G(2).

A second equally possible conformational state could be a modified $\gamma$-turn [3 → 1 between Q(5) and G(3)]. The crystal structure of cyclo[D-Phe(1)-Pro(2)-Gly(3)-D-Ala(4)-Pro(5)] has been solved and indicates that the D-Ala(4)-Pro(5)-D-Phe(1) sequence is a $\gamma$-turn [3 → 1 between D-Phe(1) and D-Ala(4)] with an $i + 1$ $\phi$, $\psi$ (−82°, +59°) torsion angle orientation (31). Theoretical calculations have indicated that the $\gamma$-turn $\phi$, $\psi$ dihedral angles could range from 75° → 85° and 60° → 70°, respectively, with the signs of the angles being +/− or −/+ (32). It is certainly possible that there may be deviations from these torsional angles in the conformationally averaged solution structure of the heptapeptide currently under study.

Inadequately resolved dipolar connectivities in the

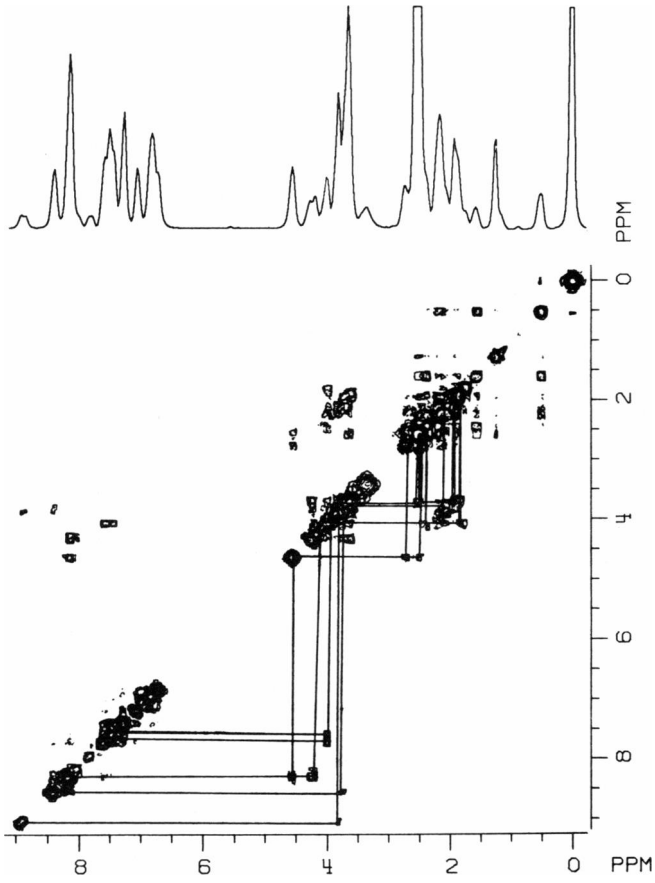


FIGURE 2 The 360 MHz $^1$H-NMR COSY contour plot of the $NH_2$-Q(1)-G(2)-G(3)-N(4)-Q(5)-S(6)-Q(7)-$CONH_2$ heptapeptide sequence around the *N*-glycosylation site of the proline-rich glycoprotein from human parotid saliva. Spin system connectivities are indicated by solid lines drawn orthogonal to the chemical shift axes. The one-dimensional NMR plot obtained by projection through $\omega_1$ is shown at the top of the COSY map. The resonances at high field (between 2 → 0 ppm) arise from the DSS.

NOESY experiments failed to provide conclusive evidence concerning the spacial arrangement(s) of the heptapeptide (30).

## NMR Analysis of the Heptapeptide $\chi_1$ Torsion Angles

The rotamer populations about $\chi_1$ were calculated using the method of Feeney (33). Table III lists the $^3J_{C^\alpha H^\alpha, C^\beta H^\beta}$ coupling constants obtained from the high-resolution one-dimensional NMR spectra of the heptamer at 30° C, the resulting fractional rotamer populations calculated from these data, and the free energy differences between the rotamer states. In each case the *gauche*$^-$ rotamer population was found to account for approximately half of the staggered rotational states, while the *trans* isomer contributed roughly one-third of the population. The remaining fraction was composed of the *gauche*$^+$ rotamer. The $\Delta F$ values provide a quantitative estimate of the stability of each rotamer population relative to one another. The rotamer populations and the corresponding $\Delta F$ values have at least one important implication. Specifically, the orientations of the amino acid side chains are directed away from the peptide backbone involved in the turn sequence presumably to minimize stereochemical interference. This conclusion was further substantiated by conventional ORTEP (20) drawings assuming a $\beta$-turn with the *gauche*$^+$ rotamer populations set as the predominant species. In these cases the amino acid side chains came in very close contact with one another and actually protruded into the turn's conformational space (i.e., the volume element defined by other atoms in the turn).

Bush et al. (34) used the model compounds 2-acetamido-1-*N*-(4-L-aspartyl)-2-deoxy-$\beta$-D-glycopyranosylamine and 1-*N*-acetyl-2-deoxy-2-acetamido-$\beta$-D-glycopyranosylamine for the investigation of the carbohydrate $\tau_1$ and $\tau_2$ dihedral angles ($\tau_1$ and $\tau_2$ describe rotations about the exocyclic amide bonds at carbons 1 and 2). Additionally, the $\chi_1$ and $\chi_2$ peptide torsional angles were elucidated. The circular dichroism and NMR results indicated that $\tau_1 = \tau_2 = +120°$ and $\chi_1 = \chi_2 = +60°$ and that the *N*-acetyl-glucosamine residue was in the $^4C_1$ form. Also, the glycosylated Asn residue was assigned to the second corner position of a type I $\beta$-turn. Beeley (35) has shown that in 30 of 31 model cases some type of $\beta$-turn exists in the vicinity of the *N*-glycosylation site. Additionally, both Beeley (35) and Aubert et al. (36) state that the second corner position of the $\beta$-turn is the most likely spot for *N*-glycosylation to occur. Further, when Asn occupies the second corner position of a $\beta$-turn, out of the two most commonly found $\beta$-turn forms (i.e., type I and type II), the type I $\beta$-turn is expected to predominate (37, 38). The general conclusion concerning the location of the Asn residue in a turn sequence is in agreement with the possible conformations elucidated in the present study. However, the peptide side-chain torsion angle populations obtained from Bush's data are not in agreement with our results. Ishii et al. (39–41) have done several NMR and circular dichroism studies of the Asp monomer, Asn-containing peptides and their glycosylated derivatives, and tetrapeptide $\beta$-turn models containing Asp and Lys. In all cases, regardless of solvent choice (i.e., aqueous versus organic), pH, amino acid sequence effects, the presence or absence of *N*-linked carbohydrate moieties, or whether Pachler's (42) or Feeney's (33) rotamer calculation method was used, the *gauche*$^-$ rotamer was found to predominate for the Asx residue. Our data closely parallel the results of Ishii et al. not only in the qualitative, but the quantitative sense as well. Overall these results indicate that the dominance of the *gauche*$^-$ rotamer population for Asx is present at the monomer level and continues through to an intact turn sequence. Apparently, this feature is not a result of higher order secondary structure or carbohydrate substitution, but rather a fundamental physical property of the Asx residue. Further, this seems to be the general trend for the remaining amino acids in our heptapeptide. Whether this

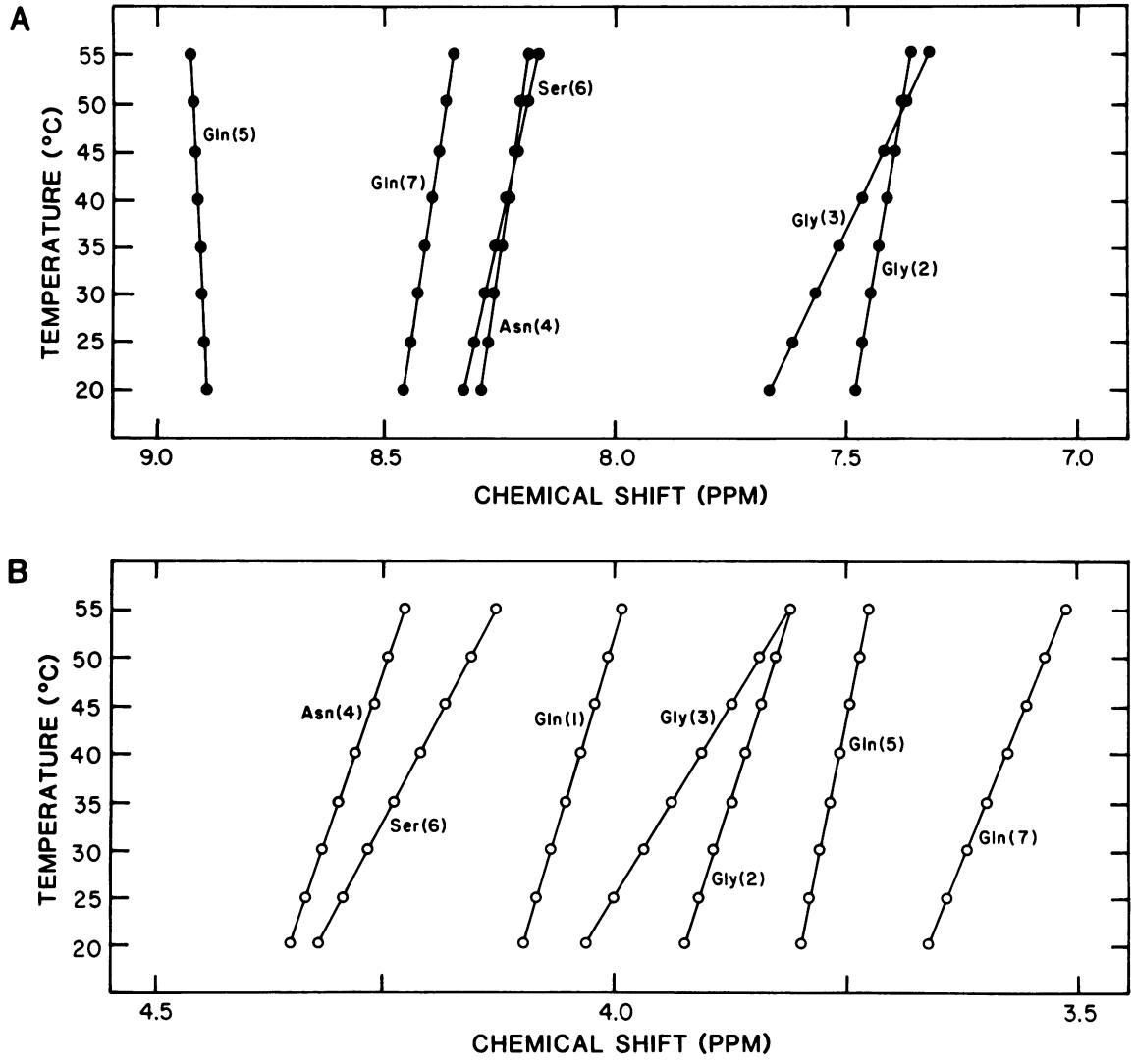


FIGURE 3 Plots of the chemical shift dependence of the (*A*) NH-backbone protons and (*B*) $C^{\alpha}H^{\alpha}$ protons for the $NH_2$-Q(1)-G(2)-G(3)-N(4)-Q(5)-S(6)-Q(7)-$CONH_2$ heptapeptide. The linear nature of the curves in *B* indicates no significant change in apparent structure over the temperature range studied (21). The slope of the curve for Gln(5) in (*A*) is indicative of a hydrogen bond (22, 23).

TABLE I
CHEMICAL SHIFTS* AND AMIDE BACKBONE PROTON TEMPERATURE DEPENDENCE‡ OF THE $NH_2$-Q(1)-G(2)-G(3)-N(4)-Q(5)-S(6)-Q(7)-$CONH_2$ PEPTIDE

| Amino acid | δ (NH) | δ ($C^{\alpha}H^{\alpha}$) | δ ($C^{\beta}H^{\beta}$) | δ ($C^{\gamma}H^{\gamma}$) | Δδ/ΔT |
|---|---|---|---|---|---|
| Gln (1) | — | 4.09 | 2.19<br>2.07 | 2.52 | — |
| Gly (2) | 7.45 | 3.89§ | — | — | − 3.4 |
| Gly (3) | 7.57 | 3.97§ | — | — | −10.0 |
| Asn (4) | 8.26 | 4.31 | 2.53<br>2.42 | — | − 2.7 |
| Gln (5) | 8.90 | 3.78 | 2.14<br>1.99 | 2.42 | + 0.8 |
| Ser (6) | 8.28 | 4.29 | 3.89 | — | − 4.6 |
| Gln (7) | 8.42 | 3.61 | 2.23<br>1.96 | 2.38 | − 3.8 |

*Chemical shifts are reported in parts per million (ppm) downfield from internal 2,2-dimethyl-2-silapentane-5-sulfonate (DSS).
‡The temperature dependence of the NH protons are reported as parts per billion (ppb) per degree Kelvin.
§The $C^{\alpha}H^{\alpha}$ and "R" group hydrogens for glycine were not distinguishable. We report here the average value of their chemical shifts.

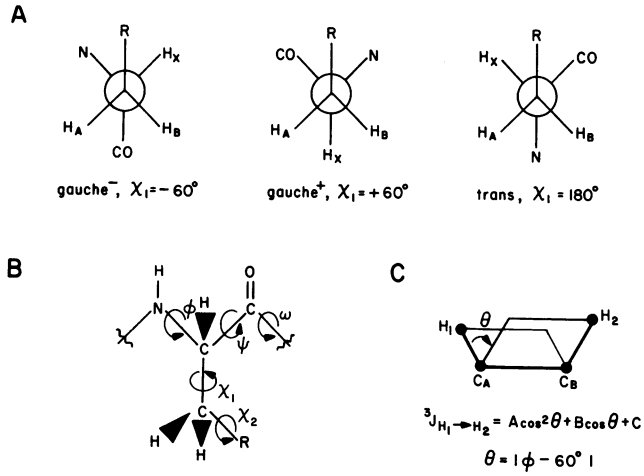


FIGURE 4 Definitions of (*A*) the amino acid side chain $\chi_1(C^\alpha - C^\beta)$ dihedral angle rotamer populations, (*B*) the $\phi(N - C^\alpha)$, $\psi(C^\alpha - CO)$, $\omega(CO - N)$, and $\chi_1(C^\alpha - C^\beta)$ peptide torsion angles and (C) the angle $\theta$ defined by the Karplus Equation (26, 27) and its conversion to $\phi$.

is also a general feature of these amino acids under a variety of environmental influences similar to those for Asx remains to be determined.

## Computer Analysis of Heptapeptide Structure

The complete definitions of all $\phi$, $\psi$, $\omega$, and $\chi$ torsion angles in the heptapeptide are diagramed in Fig. 6. The nomenclature specified in this figure should be used when referring to the calculated dihedral angles generated by the ECEPP/2-VAO4A program.

The calculation of total conformational peptide potential energy ($U_{TOT}$) was accomplished using contributions from electrostatic ($U_{EES}$), nonbonded ($U_{ENB}$) (including hydrogen-bonding energy), and torsional ($U_{ETOR}$) energies.

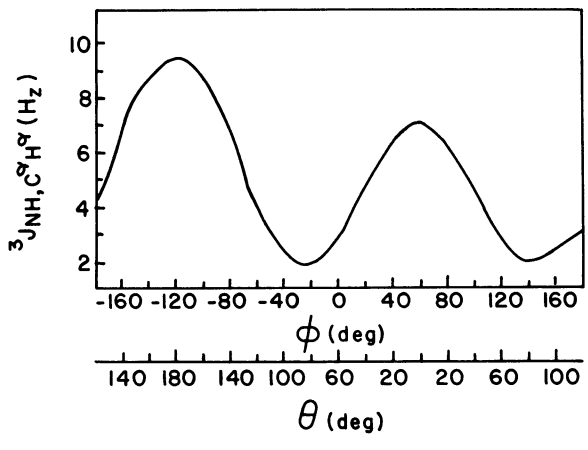


FIGURE 5 Plot of the Karplus Equation $[^3J_{NH,C^\alpha H^\alpha} = \mathbf{A}\cos^2\theta + \mathbf{B}\cos\theta + \mathbf{C}]$ (26, 27) with $\mathbf{A} = 6.4$, $\mathbf{B} = -1.4$, and $\mathbf{C} = 1.9$ (28) used to determine the $\phi(N - C^\alpha)$ peptide dihedral angle. This figure is reproduced by the kind permission of Academic Press, Inc. (London) and Dr. Kurt Wuthrich.

TABLE II
$^3J_{NH,C^\alpha H^\alpha}$ COUPLING CONSTANTS*, THE KARPLUS EQUATION $\theta$ VALUES‡, AND THE $\phi$ DIHEDRAL ANGLES§ FOR THE $NH_2$-Q(1)-G(2)-G(3)-N(4)-Q(5)-S(6)-Q(7)-$CONH_2$ PEPTIDE

| Amino acid | $^3J_{NH,C^\alpha H^\alpha}$ | $\theta$ | $\phi$ | |
|---|---|---|---|---|
| | | *degrees* | *degrees* | *degrees* |
| Gln (1) | — | — | — | — |
| Gly (2) | — | — | — | — |
| Gly (3) | — | — | — | — |
| Asn (4) | 8.09 | +151.6 | − 91.6, | −148.4 |
| | | ‖ | — | — |
| Gln (5) | 4.08 | +119.0 | +179.0, | − 59.0 |
| | | + 45.3 | + 14.7, | +105.3 |
| Ser (6) | 3.99 | +118.2 | +178.2, | − 58.2 |
| | | + 46.3 | + 13.7, | +106.3 |
| Gln (7) | 4.39 | +121.6 | −178.8, | − 61.6 |
| | | + 42.0 | + 18.0, | +102.0 |

*Observed coupling constant values are reported in Hertz.

‡The Karplus Equation (26, 27) is of the form $^3J_{NH,C^\alpha H^\alpha} = \mathbf{A}\cos^2\theta + \mathbf{B}\cos\theta + \mathbf{C}$, where the constants chosen are from Pardi et al. (28) such that $\mathbf{A} = 6.4$, $\mathbf{B} = -1.4$, and $\mathbf{C} = 1.9$. Note that this particular form of the Karplus Equation was determined by correlating observed high-resolution $^3J_{NH,C^\alpha H^\alpha}$ coupling constants in basic pancreatic trypsin inhibitor (BPTI) with the $\phi(NH\text{-}C^\alpha H^\alpha)$ dihedral angles obtained from x-ray crystallographic data. Electronegativity effects are thus accounted for as an intrinsic part of this Karplus relationship, thus allowing the use of empirical data without the need for further corrections based on a priori assumptions arising from models not using authentic amino acids in a native protein.

§The NH-$C^\alpha H^\alpha$ dihedral angle $\phi$ is defined as $\theta = |\phi - 60°|$ (24, 25).

‖The maximum $\theta$ value on the positive side of the $\phi$ portion of the Karplus Equation (see Fig. 4) is 6.90 Hz at $\theta = 0°$. Therefore the $\theta = +151.6°$ solution is unique.

Briefly paraphrasing from Scheraga's QCPE program (18), the $U_{EES}$ term arises from a Coulomb potential between two atom-centered monopole charges, $q_i$ and $q_j$

$$U_{\text{electrostatic}} = 332.0\, q_i q_j / D r_{ij}, \tag{2}$$

where $D$ is the dielectric constant (=2.0) and $r_{ij}$ is the internuclear distance between $q_i$ and $q_j$ in angstroms. The $q$ values in the ECEPP/2 program are estimated from the overlap-normalized CNDO/2 (molecular calculations with Complete Neglect of Differential Overlap) (43) charges. The $U_{ENB}$ term comes from a modified Lennard-Jones 6–12 function

$$U_{\text{nonbonded}} = F A^{kl}/r_{ij}^{12} - C^{kl}/r_{ij}^{6}, \tag{3}$$

where $F = 0.5$ or 1.0 for 1–4 or 1–5 interactions, respectively, and $A^{kl}$ and $C^{kl}$ are energy terms related to the internuclear distance $r_{ij} = r_0$ and the depth of the energy minima. The hydrogen-bonding portion of $U_{ENB}$ is given by a potential energy function as follows

$$U_{\text{hydrogen-bonding}} = A'_{HX}/r_{HX}^{12} - B_{HX}/r_{HX}^{10}, \tag{4}$$

where $A'_{HX}$ and $B_{HX}$ are energy coefficients based on the specific nuclei involved in the hydrogen-bonding scheme.

TABLE III

$^3J_{C^\alpha H^\alpha, C^\beta H^\beta}$ COUPLING CONSTANTS, THE *TRANS*, *GAUCHE*$^-$, AND *GAUCHE*$^+$ ROTAMER POPULATIONS AND THEIR FREE ENERGY DIFFERENCES FOR THE $NH_2$-Q(1)-G(2)-G(3)-N(4)-Q(5)-S(6)-Q(7)-$CONH_2$ PEPTIDE

| Amino acid | $^3J_{C^\alpha H^\alpha, C^\beta H^\beta}$§ | Rotamer populations* | | | Free energy differences‡ | | |
|---|---|---|---|---|---|---|---|
| | | *trans* | *gauche*$^-$ | *gauche*$^+$ | $\Delta F_{g^-,t}$ | $\Delta F_{t,g^+}$ | $\Delta F_{g^-,g^+}$ |
| Gln (1) | 7.47<br>4.55 | 0.34 | 0.50 | 0.16 | 232 | 454 | 686 |
| Gly (2) | — | — | — | — | — | — | — |
| Gly (3) | — | — | — | — | — | — | — |
| Asn (4) | 7.66<br>4.27 | 0.35 | 0.52 | 0.13 | 238 | 597 | 835 |
| Gln (5) | 7.80<br>4.21 | 0.33 | 0.54 | 0.13 | 297 | 561 | 858 |
| Ser (6) | — | — | — | — | — | — | — |
| Gln (7) | 7.61<br>4.35 | 0.34 | 0.52 | 0.14 | 256 | 535 | 791 |

*The rotamer populations are defined in accordance with IUPAC-IUB (24) nomenclature and the definitions of Bystrov (25). When $C^\alpha$ is behind $C^\beta$ (for example, the $\chi_1$ bond), and $C^\gamma$ is eclipsed relative to N, then $\chi_1 = 0°$. The *trans* isomer is thus defined by $\chi_1 = +180°$, while *gauche*$^-$ and *gauche*$^+$ are given by $\chi_1 = -60°$ and $+60°$, respectively. Referring to Fig. 4, the "R" would be $C^\gamma$ and $H_x$, the $C^\alpha$ proton. Thus, for $\chi_1 = +180°$ (*trans*) $\theta$[H(X), H(A) = $+60°$ and H(X), H(B) = $+180°$], for $\chi_1 = +60°$ (*gauche*$^+$) $\theta$[H(X), H(A) = $+60°$ and H(X), H(B) = $+60°$], and for $\chi_1 = -60°$ (*gauche*$^-$) $\theta$[H(X), H(A) = $+180°$, and H(X), H(B) = $+60°$]. Rotamer populations were calculated based on the equations reported by Feeney (33)

$$J_{AX} = 4.1\,p_I + 11.7\,p_{II} + 2.9\,p_{III},\ J_{BX} = 12.0\,p_I + 2.1\,p_{II} + 4.7\,p_{III},\ p_I + p_{II} + p_{III} = 1.0,$$

where $p_I$ = *trans*, $p_{II}$ = *gauche*$^-$ and $p_{III}$ = *gauche*$^+$.

‡The free energy differences between rotational states (for example, $\Delta F_{g^-,t} = F_{g^-} - F_t$; $\Delta F_{t,g^+} = F_t - F_{g^+}$; $\Delta F_{g^-,g^+} = F_{g^-} - F_{g^+}$) are calculated from the equations reported by Bystrov (25): *gauche*$^-$/*trans* = $\exp(-\Delta F_{g^-,t}/RT)$, *trans*/*gauche*$^+$ = $\exp(-\Delta F_{t,g^+}/RT)$, *gauche*$^-$/*gauche*$^+$ = $\exp(-\Delta F_{g^-,t}/RT)$. The temperature value used is 30°C (303.16 K) with $R$ = 1.98717 cal $-$ $K^{-1}$ $-$ $mol^{-1}$. The free energy differences are reported in cal-$mol^{-1}$.

§Coupling constants are reported in Hz. The low-field proton was assigned as $H_A$ (for example, $J_{AX}$ on top) and the high-field proton was assigned as $H_B$ (for example, $J_{BX}$ on the bottom) in keeping with Feeney's notation (33).

Lastly, the $U_{ETOR}$ term is generated for variable $\chi$ and $\omega$ dihedral angles from the function:

$$U_{torsional} = (U_0)(1 \pm \cos n\theta), \qquad (5)$$

where the energy difference between $U_{ESS} + U_{ENB}$ and the experimental barrier height is $U_0$, $n$ is the symmetry factor for the energy barrier, and $\theta$ is the dihedral angle in degrees. For further explanations of the energy components and the methods by which ECEPP/2 functions, the reader should see Sheraga's QCPE program (18) and references therein.

The first set of input data used for the type I $\beta$-turn model was all $\omega = +180°$, all $\chi = 60°$, $\phi_3,\psi_3 = (-60°, -30°)$, $\phi_4,\psi_4 = (-91.6°, 0°)$ and all other $\phi$, $\psi$ = $(+180°, +180°)$. The type II′ $\beta$-turn basis set used $\phi_3,\psi_3$ = $(+60°, -120°)$ with all other angles the same as the type I $\beta$-turn. The same basis set was used for the $\gamma$-turn model except that $\phi_3,\psi_3 = (+180°, +180°)$ and $\phi_4,\psi_4$ = $(-91.6°, +59°)$. All of the angles except $\phi_3,\psi_3$ and $\phi_4,\psi_4$ in the $\beta$-turn cases, or $\phi_4,\psi_4$ in the $\gamma$-turn model, were allowed to vary with large incremental differences to produce searches for global energy minima. Under 20 iteration sets were required to reach convergence in each model. The results indicated minimum energy structures where the $NH_2$ functional groups formed intramolecular hydrogen bonds with the carbonyl moieties in the peptide chain. This

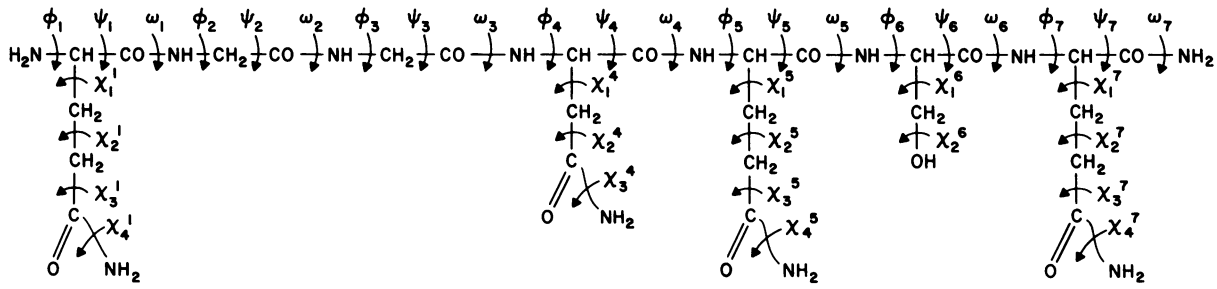


FIGURE 6 The complete definitions of all $\phi$, $\psi$, $\omega$, and $\chi$ dihedral angles in the $NH_2$-Q(1)-G(2)-G(3)-N(4)-Q(5)-S(6)-Q(7)-$CONH_2$ heptapeptide sequence around the *N*-glycosylation site of the proline-rich glycoprotein from human parotid saliva. These dihedral angles should be referred to when examining Table IV.

was accomplished by altering $\omega$ to have values intermediate between 0° and 180°. This would represent a violation of planarity for the *cis* or *trans* type bonds commonly observed in the peptide chain.

Based on the results for the global energy minimum search, certain tacit assumptions were incorporated into the minimization procedure. First, all $\omega$'s were fixed at +180° to preserve the most common planar bond type (*trans*). Second, the NMR data from Table II were used to fix the values for $\phi_5 \rightarrow \phi_7$. These data generated 12 sets (i.e., four sets each from three turn types) of minimized functions in under 20 iterations. In all cases the C—C bonds from the amino acid side chains were found to be within a few degrees of −60°.

Using the data from the second energy minimization run, one last assumption was made. The $\chi$ rotamer populations involving C—C bonds are expected to fall into one of three minimum energy solution conformations as described by Feeney (33) and listed in Table III. Therefore, since −60° was found to be a reasonable value for these angles, they were fixed in the *gauche*$^-$ conformation. Under 10 iteration sets yielded convergence with all turn models. Table IV gives the final tabulation of dihedral angles resulting from both NMR data and energy minimization procedures. Figs. 7–9 illustrate the ORTEP (20) drawings of the $\gamma$- and $\beta$-turns resulting from the data in Table IV.

The internuclear distances between the amide backbone proton/nitrogen of Q(5) and the backbone carbonyl moiety of G(2) are 1.81/2.62 Å and 1.79/2.71 Å for the type I and type II′ $\beta$-turns, respectively. The corresponding Q(5) → G(3) bond distances for the $\gamma$-turn are 2.27/3.09 Å. From these distance criteria it can be seen that the $\beta$-turn models have strong intramolecular hydrogen bonds while the $\gamma$-turn has a weaker hydrogen bond. This would argue in favor of the $\beta$-turns as being more likely in view of the NMR amide proton chemical shift versus temperature data. Also, the type I $\beta$-turn, type II′ $\beta$-turn and $\gamma$-turn have total potential energies of +142, −6 and −28 kcal/mol, respectively. These data imply the type I $\beta$-turn is highly unstable, whereas the type II′ $\beta$-turn and $\gamma$-turn are energetically favored. Taken together, these factors suggest the type II′ $\beta$-turn best fits the NMR data, energetic considerations and internuclear hydrogen-bonding data presented in this study.

## CONCLUSIONS

The solution conformation of nearly all small linear peptides is expected to be a mixture of two or more conformational states. In the present case, the strong hydrogen-bond acceptor DMSO was used as the solvent medium and found to stabilize at least one of the model heptapeptide conformations sufficiently to give rise to an observable population of turn sequence(s) on the NMR time scale. In

TABLE IV
CALCULATED* DIHEDRAL ANGLES FOR THE TYPE I AND TYPE II′ $\beta$-TURNS AND $\gamma$-TURN PREDICTED FOR THE $NH_2$-Q(1)-G(2)-G(3)-N(4)-Q(5)-S(6)-Q(7)-$CONH_2$ PEPTIDE

| Amino acid | Dihedral angles‡ | | | | | | |
|---|---|---|---|---|---|---|---|
| | $\phi$ | $\psi$ | $\omega$ | $\chi_1$ | $\chi_2$ | $\chi_3$ | $\chi_4$ |
| Gln (1) | −65.6 | 142.0 | 180.0 | −60.0 | −60.0 | −60.0 | −84.7 |
| | −73.7 | 149.8 | 180.0 | −60.0 | −60.0 | −60.0 | −80.6 |
| | −74.4 | 150.2 | 180.0 | −60.0 | −60.0 | −60.0 | −80.5 |
| Gly (2) | 175.1 | 140.0 | 180.0 | | | | |
| | −177.4 | −130.0 | 180.0 | | | | |
| | −160.3 | 141.2 | 180.0 | | | | |
| Gly (3) | −60.0 | −30.0 | 180.0 | | | | |
| | 60.0 | −120.0 | 180.0 | | | | |
| | 141.3 | −124.0 | 180.0 | | | | |
| Asn (4) | −91.6 | 0.0 | 180.0 | −60.0 | −60.0 | −82.8 | |
| | −91.6 | 0.0 | 180.0 | −60.0 | −60.0 | −82.9 | |
| | −91.6 | 59.0 | 180.0 | −60.0 | −60.0 | −83.5 | |
| Gln (5) | −59.0 | 164.3 | 180.0 | −60.0 | −60.0 | −60.0 | 109.1 |
| | −59.0 | 148.4 | 180.0 | −60.0 | −60.0 | −60.0 | −72.0 |
| | −59.0 | 147.7 | 180.0 | −60.0 | −60.0 | −60.0 | −91.6 |
| Ser (6) | −58.2 | 102.0 | 180.0 | −60.0 | 178.4 | | |
| | −58.2 | 124.3 | 180.0 | −60.0 | 178.4 | | |
| | −58.2 | 114.3 | 180.0 | −60.0 | 178.4 | | |
| Gln (7) | −61.6 | 147.6 | 180.0 | −60.0 | −60.0 | −60.0 | −64.0 |
| | −61.6 | 149.0 | 180.0 | −60.0 | −60.0 | −60.0 | 122.9 |
| | −61.6 | 149.0 | 180.0 | −60.0 | −60.0 | −60.0 | 122.8 |

*Calculated from ECEPP/2 – VAO4A (18, 19) based on the NMR data from Tables II and III. See the text for details on procedure.
‡The data are presented as type I $\beta$-turn (*top*) ($U_{TOT}$ = +142 kcal/mol), type II′ $\beta$-turn (*middle*) ($U_{TOT}$ = −6 kcal/mol) and $\gamma$-turn (*bottom*) ($U_{TOT}$ = −28 kcal/mol).

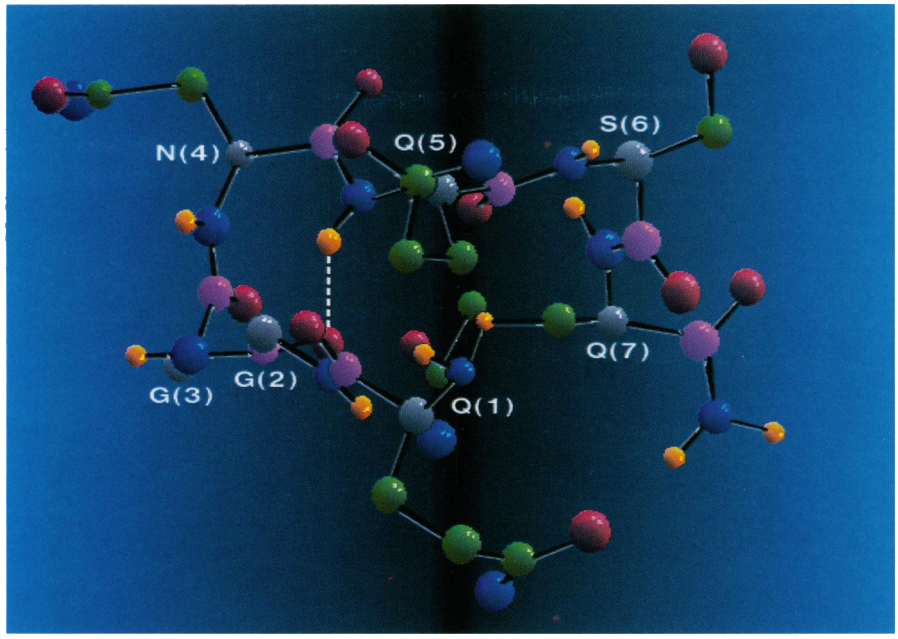


FIGURE 7 The color enhanced ORTEP (20) rendering (Oceana) of the type I $\beta$-turn in the $NH_2$-Q(1)-G(2)-G(3)-N(4)-Q(5)-S(6)-Q(7)-$CONH_2$ heptapeptide based on the data in Table IV. Except for the amide peptide backbone protons, no hydrogens are shown. Atoms are represented as follows: *blue*, nitrogen; *yellow*, hydrogen; *grey*, peptide backbone alpha carbon; *green*, amino acid functional group carbon; *pink*, carbonyl peptide backbone carbon; *red*, oxygen. The dashed line represents a hydrogen bond.

general, the observation of stable peptide conformations in DMSO is not novel, though, since the literature has many such examples of non-random peptide structures found in both water and DMSO (see, for example, references 21–23, 44, and 45). The heptapeptide conformations presented in the present study, however, are strongly solvent dependent. Our findings from circular dichroism spectroscopy of the heptapeptide in an aqueous environment (46) indicate that there are different populations of turn(s) present at varying pH's. Thus, in both DMSO and water the presence of turn-type conformations for this heptapeptide has been demonstrated.

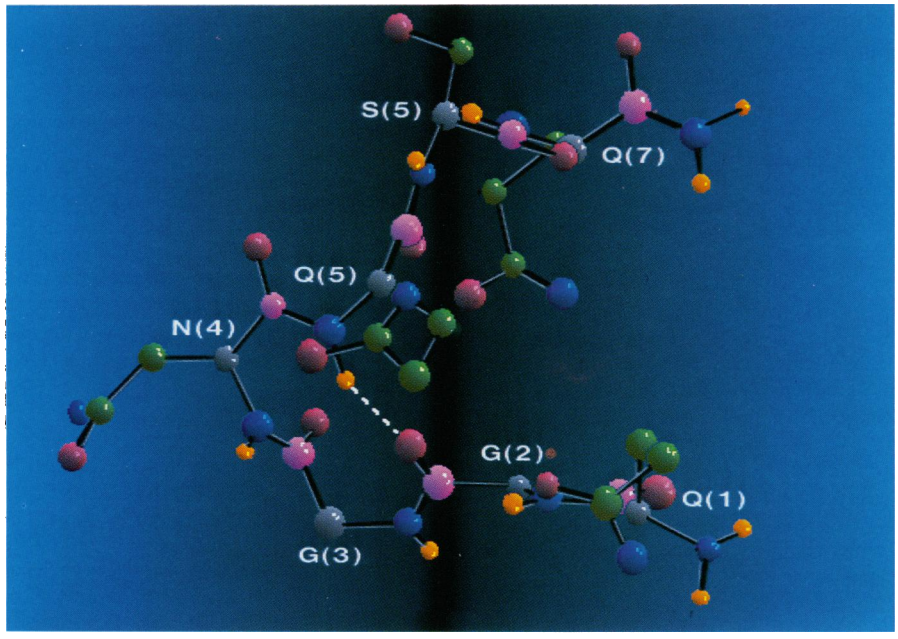


FIGURE 8 The color enhanced ORTEP (20) rendering (Oceana) of the Type II' $\beta$-turn in the $NH_2$-Q(1)-G(2)-G(3)-N(4)-Q(5)-S(6)-Q(7)-$CONH_2$ heptapeptide based on the data in Table IV. See the legend in Fig. 7 for further details.

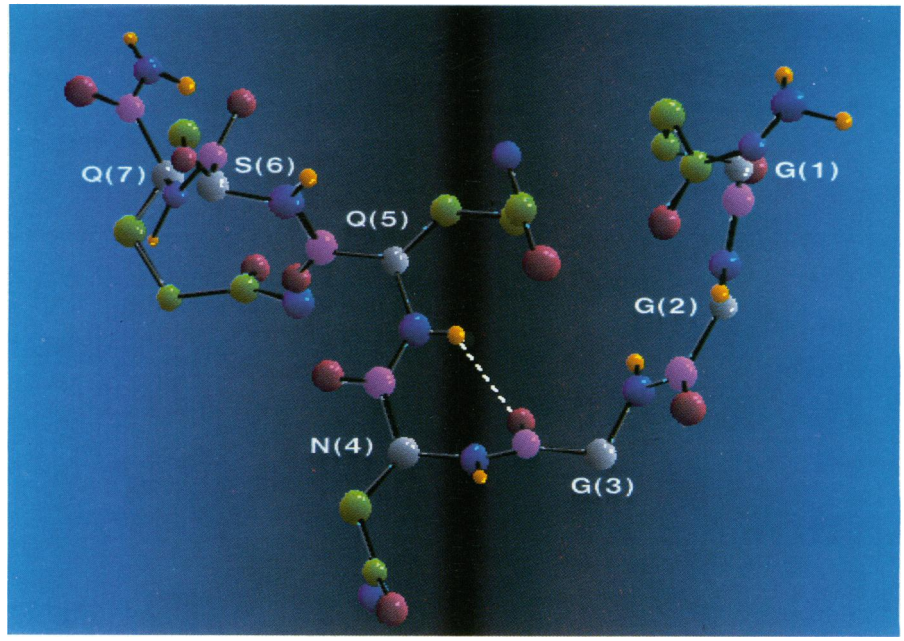


FIGURE 9 The color enhanced ORTEP (20) rendering (Oceana) of the γ-turn in the $NH_2$-Q(1)-G(2)-G(3)-N(4)-Q(5)-S(6)-Q(7)-$CONH_2$ heptapeptide based on the data in Table IV. See the legend in Fig. 7 for further details.

Globular protein structures can be stabilized by a variety of forces such as hydrophobic interactions, disulfide bridges, specific solvent interactions, long- and short-range hydrogen-bonding schemes, salt bridges, and aromatic interactions. The turn sequences in globular proteins thus have available several types of stabilizing influences derived from the macromolecule's tertiary structure. Since our previous studies have indicated a lack of organized tertiary structure in PRG (11), one might expect those amino acid sequences involved in turns to possess properties that make them stable to the physiological conditions of the oral cavity. This may be especially true for the *N*-glycosylation sites in PRG since there is evidence that the presence of a β-turn with Asn in the $i + 2$ position may be a general stereospecific requirement for post-translational glycosylation to occur in *N*-linked glycoproteins (46–49).

The authors would like to thank the following individuals for their participation in this work: Mr. Lou Rera and Mr. Mark Rand of OCEANA for their artistic guidance and preparation of the color renderings of ORTEP; OCS Laboratories for working with us to prepare the heptapeptide; Mr. Robert Dunford for invaluable assistance in implementing the ECEPP/2-VAO4A program; Mr. Hector Velasco for preparation of manuscript figures; Mrs. Pamela M. Loomis and Dr. Pamela C. Jones for help in the preparation of this manuscript. R. E. Loomis would also like to thank the SUNY Buffalo Health-Care Instruments and Device Institute (HIDI) Grant committee for awarding funds to support our computer simulations in this project.

This work was supported by U.S. Public Health Service Grants DE07760, DE04518, DE04971, GM22490, and HIDI Grant 15O-Q009D.

*Received for publication 31 March 1986 and in final form 17 September 1986.*

## REFERENCES

1. Li, H. C., and M. J. Levine, 1980. Characterization of a glycopeptide from the proline-rich glycoprotein of human parotid saliva. *Arch. Oral Biol.* 25:353–355.
2. Shimomura, H., Y. Kanai, and K. Sanada. 1983. Amino acid sequences of glycopeptides obtained from basic proline-rich glycoprotein of human parotid saliva. *J. Biochem.* 93:857–863.
3. Maeda, N., H. -S. Kim, E. A. Azen, and O. Smithies. 1985. Differential RNA splicing and post-translational cleavages in the human salivary proline-rich protein gene system. *J. Biol. Chem.* 260:11123–11130.
4. Reddy, M. S., M. J. Levine, and L. A. Tabak. 1982. Structure of the carbohydrate chains of the proline-rich glycoprotein from human parotid saliva. *Biochem. Biophys. Res. Commun.* 104:882–888.
5. Bryan, A. R., L. A. Tabak, M. J. Levine, R. E. Cohen, and G. H. Nancollas. 1984. Adsorption of human proline-rich glycoprotein to hydroxyapatite. *J. Dent. Res.* 63:657 (Abstr.)
6. Levine, M. J., L. A. Tabak, M. S. Reddy, and I. D. Mandel. 1985. Nature of salivary pellicles in microbial adherence: role of salivary mucins. *In* Molecular Basis of Oral Microbial Adhesion. S. Mergenhagen and B. Rosan, editors. American Society of Microbiology, Washington, DC. 125–130.
7. Hatton, M. N., R. E. Loomis, M. J. Levine, and L. A. Tabak. 1985. Masticatory lubrication: the role of carbohydrate in the lubricating property of a salivary-albumin complex. *Biochem. J.* 230:817–820.
8. Shibata, S., K. Nagata, R. Nakumura, A. Tsunemitsu, and A. Misaki. 1980. Interaction of parotid saliva basic glycoprotein with *Streptococcus sanguis* ATCC 10557. *J. Periodontol.* 51:499–504.
9. Stinson, M. W., R. P. Dittmer, M. J. Levine, L. A. Tabak, P. A. Prakobphol, P. A. Murray, and M. S. Reddy. 1983. Adherence of *Streptococcus sanguis* to salivary proline-rich glycoprotein-coated glass. *J. Dent. Res.* 62:960. (Abstr).
10. Bergey, E. J., M. J. Levine, M. S. Reddy, S. D. Bradway, and I. Al-Hashimi. 1986. Use of the photoaffinity cross-linking agent *N*-hydroxylsuccinimidyl-4-azidosalicylic acid to characterize salivary-glycoprotein-bacterial interactions. *Biochem. J.* 234:43–48.
11. Loomis, R. E., E. J. Bergey, M. J. Levine, and L. A. Tabak. 1985.

Circular dichroism and fluorescence analyses of a proline-rich glycoprotein from human parotid saliva. *Int. J. Pept. Protein Res.* 26:621–629.

12. Loomis, R. E., C. C. Tseng, and M. J. Levine. 1986. Dynamics of a proline-rich glycoprotein from human parotid saliva: a 360-MHz proton nuclear magnetic resonance investigation. *Int. J. Biol. Macromol.* 8:149–152.
13. Bax, A., and R. Freeman. 1981. Investigation of complex networks of spin-spin couplings by two-dimensional NMR. *J. Magn. Reson.* 44:542–561.
14. States, D. J., R. A. Haberkorn, and D. J. Ruben. 1982. A two-dimensional nuclear overhauser experiment with pure absorption phase in four quadrants. *J. Magn. Reson.* 48:286–292.
15. Wynants, C., G. Van Binst, and H. R. Loosli. 1985. SMS 201-995, a very potent analog of somatostatin: assignment of the $^1$H 500 MHz N.M.R. spectra and conformational analysis in aqueous solution. *Int. J. Pept. Protein Res.* 25:608–614.
16. Kumar, A., R. R. Ernst, and K. Wuthrich. 1980. A two-dimensional nuclear overhauser enhancement (2D NOE) experiment for the elucidation of complete proton-proton cross-relaxation networks in biological macromolecules. *Biochem. Biophys. Res. Commun.* 95:1–6.
17. Baumann, R., G. Wider, R. R. Ernst, and K. Wuthrich. 1981. Improvement of 2D NOE and 2D correlated spectra by symmetrization. *J. Magn. Reson.* 44:402–406.
18. Scheraga, H. A. 1982. ECEPP/2: empirical conformational energy program for peptides. *In* Quantum Chemistry Program Exchange. 454. Department of Chemistry, Indiana University, Bloomington, IN.
19. Powell, M. J. D. 1964. VA04A: Minimum of a Function of Several Variables. *In* Quantum Chemistry Program Exchange. 60. Department of Chemistry, Indiana University, Bloomington, IN.
20. Johnson, C. K. 1976. ORTEP II: FORTRAN Thermal Ellipsoid Plot Program for Crystal Structure Illustrations (third version). Oak Ridge National Laboratory, Oak Ridge, TN. ORNL–5138.
21. Miyazawa, T., and T. Higashijima. 1981. NMR analyses of linear peptides in solution. *Biopolymers.* 20:1949–1958.
22. Roques, B. P., C. Garbay-Jaureguiberry, R. Oberlin, M. Anteunius, and A. K. Lala. 1976. Conformation of Met$^5$-enkephalin determined by high field PMR spectroscopy. *Nature (Lond.).* 262:2778–779.
23. Jones, C. R., W. A. Gibbons, and V. Garsky. 1976. Proton magnetic resonance studies of conformation and flexibility of enkephalin peptides. *Nature (Lond.).* 262:779–782.
24. IUPAC-IUB Commission on Biological Nomenclature. Abbreviations and Symbols for the Description of the Conformation of Polypeptide Chains. Tentative Rules (1969). 1970. *Biochemistry.* 9:3471–3479.
25. Bystrov, V. 1976. Spin-spin coupling and the conformational states of peptide systems. *Prog. NMR Spectrosc.* 10:41–81.
26. Karplus, M. 1959. Contact electron-spin coupling of nuclear magnetic moments *J. Chem. Phys.* 30:11–15.
27. Karplus, M. 1963. Vicinal proton coupling in nuclear magnetic resonance. *J. Am. Chem. Soc.* 85:2870–2871.
28. Pardi, A., M. Billeter, and K. Wuthrich. 1984. Calibration of the angular dependence of the amide proton-C$^\alpha$ proton coupling constants, $^3J_{HN}\alpha$, in a globular protein: use of $^3J_{HN}\alpha$ for identification of helical secondary structure. *J. Mol. Biol.* 180:741–751.
29. Crisma, M., G. D. Fasman, H. Balaram, and P. Balaram. 1984. Peptide models for $\beta$-turns: a circular dichroism study. *Int. J. Pept. Protein Res.* 23:411–419.
30. Wuthrich, K., M. Billeter, and W. Braun. 1984. Polypeptide secondary structure determination by nuclear magnetic resonance observation of short proton-proton distances. *J. Mol. Biol.* 180:715–740.
31. Karle, I. L. 1978. Crystal structure and conformation of *cyclo*-(glycylprolylglycyl-D-alanylproyl) containing 4 → 1 and 3 → 1 intramolecular hydrogen bonds. *J. Am. Chem. Soc.* 100:1286–1289.
32. Venkatachalam, C. M. 1968. Stereochemical criteria for polypeptides and proteins. V. Conformation of a system of three linked peptide units. *Biopolymers.* 6:1425–1436.
33. Feeney, J. 1976. Improved component vicinal coupling constants for calculating side-chain conformations in amino acids. *J. Magn. Reson.* 21:473–478.
34. Bush, C. A., A. Duben, and S. Ralapati. 1980. Conformation of the glycopeptide linkage in asparagine-linked glycoproteins. *Biochemistry.* 19:501–504.
35. Beeley, J. G. 1977. Peptide chain conformation and the glycosylation of glycoproteins. *Biochem. Biophys. Res. Commun.* 76:1051–1055.
36. Aubert, J. M., G. Biserte, and M. H. Loucheux-Lefebvre. 1976. Carbohydrate-peptide linkage in glycoproteins. *Arch. Biochem. Biophys.* 175:410–418.
37. Kopple, K. D., and A. Go. 1977. Conformation of cyclic peptides. 9. Cyclodimerization of a hexapeptide unit at high concentration. Rationalization in terms of the conformation of the cyclic dodecapeptide. *J. Am. Chem. Soc.* 99:7698–7704.
38. Chou, P., and G. D. Fasman. 1977. $\beta$-turns in proteins. *J. Mol. Biol.* 115:135–175.
39. Ishii, H., Y. Inque, and R. Chujo. 1984. Conformational study of glycopeptides: Asn-containing peptides and their glycosylated derivatives. *Int. J. Pept. Protein Res.* 24:421–429.
40. Ishii, H., Y. Inque, and R. Chujo. 1984. $\beta$-turn-like conformation and side chain interactions of aspartic acid-containing dipeptides. *Polym. J.* 16:9–21.
41. Ishii, H., Y. Fukunishi, Y. Inque, and R. Chujo. 1984. $\beta$-turn structure and intramolecular interaction of tetrapeptides containing Asp and Lys. *Biopolymers.* 24:2045–2056.
42. Pachler, K. G. R. 1964. Nuclear magnetic resonance study of some $\alpha$-amino acids. II. Rotational isomerism. *Spectrochim. Acta. Part A. Mol. Spectrosc.* 20:581–587.
43. Segal, G. A. 1966. CNDO/2: molecular calculations with complete neglect of differential overlap. *In* Quantum Chemistry Program Exchange 91. Department of Chemistry, Indiana University, Bloomington, IN.
44. Durieux, C., J. Belleney, J. Y. Lallemand, B. P. Roques, and M. C. Fournie-Zaluski. 1983. $^1$H-NMR conformational study of sulfated and non-sulfated cholecystokinin fragment $CCK_{27-33}$: influence of the sulfate group on the peptide folding. *Biochem. Biophys. Res. Comm.* 114:705–712.
45. Fournie-Zaluski, M. C., C. Durieux, B. Lux, J. Belleney, P. Pham, D. Gerard, B. P. Roques. 1985. Conformational analysis of cholecystokinin fragments $CCK_4$, $CCK_5$, and $CCK_6$ by $^1$H-NMR spectroscopy and fluorescence-transfer measurements. *Biopolymers.* 24:1663–1681.
46. Tseng, C. -C., R. E. Loomis, E. J. Bergey, and M. J. Levine. 1986. Circular Dichroism Spectroscopy of a synthetic heptapeptide from the proline-rich glycoprotein of human parotid saliva. *J. Dent. Res.* 65:1411. (Abstr).
47. Chou, P. Y., and G. Fasman. 1979. Prediction of $\beta$-turns. *Biophys. J.* 26:367–384.
48. Bause, E., H. Hettkamp, and G. Leger. 1982. Conformational aspects of *N*-glycosylation of proteins: studies with linear and cyclic peptides as probes. *Biochem. J.* 203:761–768.
49. Bause, E. 1983. Structural requirements of *N*-glycosylation of proteins: studies with proline peptides as conformational probes. *Biochem. J.* 209:331–336.